THE JOURNAL OF PHYSICAL CHEMISTRY C
A JOURNAL OF THE AMERICAN CHEMICAL SOCIETY

pubs.acs.org/JPCC

Article

Lifetime of Photogenerated Positive Charges in Hybrid Cerium Oxide-Based Materials from Space and Mirror Charge Effects in Time-Resolved Photoemission Spectroscopy

Jacopo Stefano Pelli Cresi,* Eleonora Spurio, Lorenzo Di Mario, Patrick O'Keeffe, Stefano Turchini, Stefania Benedetti, Gian Marco Pierantozzi, Alessandro De Vita, Riccardo Cucini, Daniele Catone, and Paola Luches

Cite This: J. Phys. Chem. C 2022, 126, 11174−11181

Read Online

ACCESS | Metrics & More | Article Recommendations | Supporting Information

ABSTRACT: Space and mirror charge effects in time-resolved photoemission spectroscopy can be modeled to obtain relevant information on the recombination dynamics of charge carriers. We successfully extracted from these phenomena the reneutralization characteristic time of positive charges generated by photoexcitation in CeO_2-based films. For the above-band-gap excitation, a large fraction of positive carriers with a lifetime that exceeds 100 ps are generated. Otherwise, the sub-band-gap excitation induces the formation of a significantly smaller fraction of charges with lifetimes of tens of picoseconds, ascribed to the excitation of defect sites or to multiphoton absorption. When the oxide is combined with Ag nanoparticles, the sub-band-gap excitation of localized surface plasmon resonances leads to reneutralization times longer than 300 ps. This was interpreted by considering the electronic unbalance at the surface of the nanoparticles generated by the injection of electrons, via localized surface plasmon resonance (LSPR) decay, into CeO_2. This study represents an example of how to exploit the space charge effect in gaining access to the surface carrier dynamics in CeO_2 within the picosecond range of time, which is fundamental to describe the photocatalytic processes.

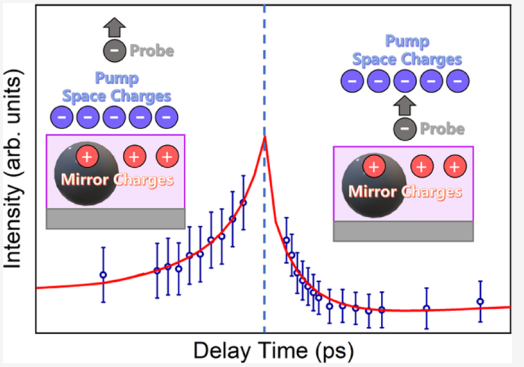

INTRODUCTION

In recent decades, the demand for active catalysts for environmental protection applications has acquired a great deal of interest, in part, due to the growing concern for global warming.[1] In this context, transition-metal oxides, such as cerium oxide (CeO_2) or titanium oxide (TiO_2), are particularly attractive, thanks to their efficiency in catalyzing redox reactions. On the other hand, these materials have poor light-induced activity in the visible range due to their wide band gaps (4.0 eV for CeO_2[2] and 3.7−3.4 eV for TiO_2[3]). Several studies have demonstrated that the combination of oxides with plasmonic metal nanoparticles (NPs), such as Au or Ag, extends their photocatalytic activity into the visible range.[4−6] The strong interaction between visible radiation and the NPs leads to the excitation of localized surface plasmon resonances (LSPRs), which induce a charge or energy transfer to the surrounding oxide, extending the spectral response range of the material.[7] A detailed description of photoexcited states in these materials is very important in view of designing materials with optimized light-induced functionalities.

Photoexcitation of CeO_2 with photons in the ultraviolet range leads to the transient occupation of localized states of the Ce 4f character, located between the valence band and the conduction band, with long lifetimes on the order of hundreds of picoseconds,[2] which may lead to a transient modification of important properties of the material like, for example, oxygen vacancy formation. When CeO_2 is coupled to Ag NPs, LSPR excitation with visible light leads to an efficient energy transfer to the oxide, inducing a dynamic response in the excited states of the oxide comparable to that observed by direct ultraviolet (UV) photoexcitation.[4,8]

Photoelectron spectroscopy (PES) is a powerful technique for the study of electronic properties in condensed matter systems. The development of free electron lasers and high harmonic generation (HHG) light sources allows the production of ultrashort radiation pulses with photon energies ranging from extreme ultraviolet to hard X-rays. The use of ultrashort pulses in time-resolved PES (trPES) experiments in the pump−probe configuration provides access to the

Received: March 29, 2022
Revised: June 15, 2022
Published: June 29, 2022

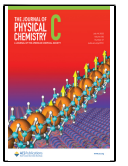

Downloaded via UNIV DEGLI STUDI DI MODENA on July 29, 2022 at 12:38:34 (UTC).
See https://pubs.acs.org/sharingguidelines for options on how to legitimately share published articles.

ACS Publications

© 2022 The Authors. Published by American Chemical Society

https://doi.org/10.1021/acs.jpcc.2c02148
J. Phys. Chem. C 2022, 126, 11174−11181

dynamics of the transient electronic structure of the investigated material on time scales typical of elementary electronic and lattice processes.[9]

However, the use of ultrashort and highly brilliant photon sources often gives rise to space charge effects, causing a significant alteration of the PES spectrum and a consequent loss of the information contained in the intrinsic photoelectron energy distribution and its temporal dynamics. Since this phenomenon represents a severe limitation for trPES experiments, wide research efforts have been dedicated to understanding and minimizing it.[10−16] Space charge effects are due to the mutual Coulomb interaction between the photoelectrons leaving the sample surface after the excitation by an ultrashort light pulse of sufficient intensity. In pump−probe trPES experiments, the intense laser pump pulse generates numerous photoelectrons that leave the surface with a spatial distribution determined by their kinetic energy. The photoelectrons generated by the far less intense probe pulse, while traveling toward the detector, interact with the space charge, which introduces, in general terms, a broadening and a shift by up to several eV of the apparent energy distribution, decreasing the effective energy resolution of the experiment and preventing the detection of important information related to pump-induced photoexcited charge dynamics. Moreover, the effect of space charge is combined with the effect of holes left behind in the sample following the emission of photoelectrons, which is often referred to as the mirror charge effect.[10,12,13] Previous investigations showed that vacuum space and mirror charge effects can be analyzed and modeled to infer important properties of the materials under investigation, in particular, to determine the lifetime of the holes photogenerated on the sample surface by the pump pulse.[10,12]

In the present study, we use the intensity variation of a specific PES feature generated by the space charge to study the dynamics of the surface pump-generated carriers in a prototypal system for photocatalysis composed of Ag NPs embedded in a CeO_2 film. The study was carried out by modeling the dynamics of the space charge effect and its effect on PES spectra. In this way, trPES can provide complementary information to UV−vis pump−probe absorption techniques, which are principally sensitive to the bulk properties of the sample and inefficient in separating the contributions of holes and electrons. Using the proposed procedure, we extracted information on the reneutralization of positive carriers in the Ag@CeO_2 system by the pump, providing a physical interpretation of the results, which is fundamental in the view of future applications in photocatalysis of the investigated systems.

METHODS

Previous studies showed that CeO_2 films grow with a comparable morphology and structure on several different single-crystal metal supports with a hexagonal surface symmetry, among which are Pt(111) and Cu(111).[17−19] Pt(111) is a substrate that we have extensively used as a support for the growth of ultrathin epitaxial cerium oxide films.[19−21] Cu(111) has also been used as a support, obtaining films with comparable surface properties, as those obtained on the Pt(111) crystal.[17] In the present study, two different samples were investigated: a CeO_2 thin layer grown on Cu(111) and a sample composed of Ag NPs embedded into a CeO_2 matrix on Pt(111). The ultrahigh vacuum (UHV) experimental apparatus used for the growth of the samples has already been described in reference 20. The metallic substrates were prepared by repeated cycles of sputtering with Ar^+ ions (1 keV, 1 μA) and annealing (1040 K for Pt(111) and 620 K for the Cu(111)) in UHV until no contaminants were revealed by in situ X-ray photoelectron spectroscopy (XPS). The CeO_2 films were grown via molecular beam epitaxy (MBE), by evaporating cerium from an electron beam evaporator, in a controlled oxygen partial pressure of 10^{-7} mbar. The substrates were kept at room temperature (RT) during sample growth. After the deposition of CeO_2 on the Pt substrate, Ag was deposited from a Knudsen cell, and, as already demonstrated,[21,22] it self-assembled into NPs on the CeO_2 surface. The growth chamber is equipped with a quartz microbalance, which was used to calibrate both the Ag and the Ce evaporators. The CeO_2 film thickness was chosen to be 2 nm to have a full coverage of the substrate surface.[20] On top of the CeO_2 film grown on Pt(111), an equivalent thickness of 1.2 nm of Ag has been evaporated. This procedure brings to the formation of self-assembled NPs, as reported in reference 23. Here, the nominal Ag thickness refers to the equivalent thickness of a uniform Ag film completely covering the ceria layer. Since the samples are grown on a highly reflective metal single crystal, it is not easy to perform an optical characterization. However, a sample grown on a transparent MgO substrate with the same procedures and the same nominal thickness has shown a very broad LSPR-related absorption band in the visible.[23] Finally, a protective capping layer of 0.5 nm CeO_2 has been added. The thickness of the uppermost CeO_2 layer was chosen to be much thinner than the bottom one to be sensitive to the interface between Ag NPs and CeO_2. The sample with Ag NPs will be referred to as Ag@CeO_2 in the following.

After the deposition of each layer, the samples were characterized in situ by steady XPS and ultraviolet photoemission spectroscopy (UPS). XPS measurements were performed with Al Kα photons from a double anode X-ray source, while the UPS spectra were acquired using a He lamp. For both acquisitions, a hemispherical electron analyzer in a normal emission geometry was used. To obtain quantitative information on the surface stoichiometry, the Ce 3d XPS spectra were fit with Voigt-shaped Ce^{3+}- and Ce^{4+}-related components, following the procedure introduced by Skala et al.[24]

The samples were transferred to the NFFA-SPRINT (Spin-Polarized Research Instrument in the Nanoscale and Time domain[25]) facility at Elettra, Trieste, to perform trPES measurements. To avoid air exposure, an ultrahigh vacuum ($P = 10^{-10}$ mbar) suitcase was used for the transfer.

The experimental apparatus used for the trPES measurements is fully described in ref 26. The system is based on a Yb:KGW-based integrated femtosecond laser system (PHAROS, Light Conversion, 1030 nm, 300 fs) with two separate amplifiers pumped by the same oscillator. This configuration guarantees a high pulse-to-pulse stability. The first amplifier is used to pump an optical parametric amplifier whose output is used to provide pump pulses. The second amplifier is used to produce high harmonics of the laser fundamental constituting the probe signal. We chose the 11th (26.5 eV) and the 13th harmonics (31.2 eV), with 5 10^6 and 10^7 photons per pulse. During the experiment, two pump energies have been used: 4.1 and 2.8 eV. The repetition rate has been set to 25 kHz, varying the energy-per-pulse between 0.3 and 1 μJ (see Table 1 for more details) concentrated on a spot size of 300 μm. Electron detection is performed with a

https://doi.org/10.1021/acs.jpcc.2c02148
J. Phys. Chem. C 2022, 126, 11174−11181

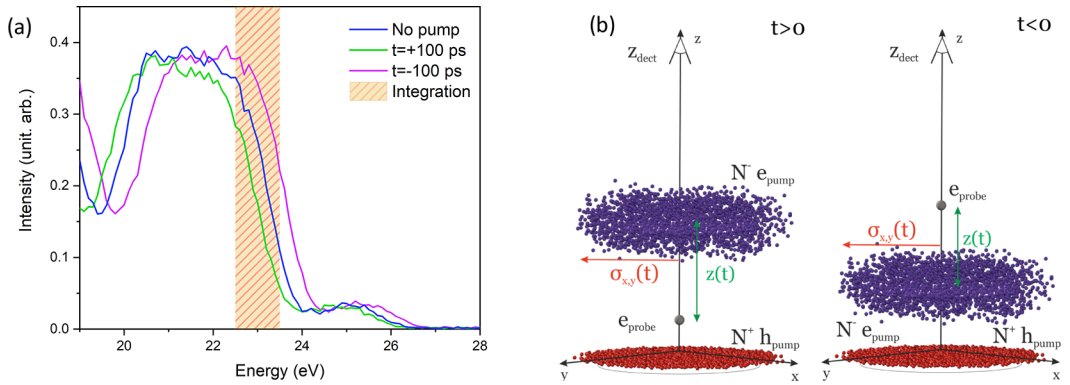

Figure 1. (a) PES spectrum of the valence band of the CeO_2 sample without the pump (blue curve) at +100 ps (green curve) and −100 ps (purple curve) delay times (pump at 4.1 eV) obtained using the HHG 13th harmonic (31.2 eV). The red box represents the energy window to which the acquisition was restricted. (b) Space charge generation (the electrons are denoted in blue and the holes are denoted in red) and its effects on the probe electron dynamics depending on $z(t)$ (the distance between the electron cloud and the probe electron).

Scienta SES 2002 hemispherical electron analyzer equipped with a phosphor detector and a charge-coupled device (CCD) camera.

The data analysis was based upon the mean-field model described by Oloff et al. in ref 12 and ref 13. One of the main approximations of the model is to assume that the cloud of electrons excited by the pump pulse has a Gaussian charge distribution in the surface plane (x and y directions) and moves along the direction normal to the surface (z direction). Moreover, the number of electrons generated by the pump pulse is assumed to be much higher than that of electrons generated by the probe. This assumption is in agreement with the conditions used for the present experiment since the drain current generated by the probe ∼2 pA was significantly lower than the pump-induced drain currents reported in Table 1.

The kinetic energy shift $\mu(t)$ experienced by a photoelectron generated by the probe pulse traveling toward the detector is due to the electric fields generated by the pump-induced electron cloud and by the positive carriers on the sample surface

$$\mu(t) = E_{k0} - E_k' = e(V^-(z(t)) - V^+(z(t))) \quad (1)$$

where E_{k0} is the unperturbed electron kinetic energy, E_k' is the perturbed one, e is the elementary charge, and V^- and $V^\pm$ are the electrostatic potentials generated by the space charge (electrons) and by the mirror charge (positive charges) measured at a distance z_{det} (analyzer aperture distance from the sample). Figure 1b reports a scheme of the space charge effect in trPES depending on z, which is correlated to the delay time t between the pump and probe.

The electrostatic potential generated by the pump-induced electron and hole clouds in the Gaussian shape approximation can be written as[27]

$$V^\pm(z(t)) = \frac{N^\pm e}{4\pi^{3/2}\varepsilon_0} \int_0^\infty \frac{\exp\left(-\frac{z(t)^2}{2\sigma_z^2 + q}\right)}{\sqrt{(2\sigma_x^2 + q)(2\sigma_y^2 + q)(2\sigma_z^2 + q)}} dq \quad (2)$$

where N^- and N^+ are, respectively, the number of photoelectrons and holes generated by the pump, e is the elementary charge, ε_0 is the vacuum permittivity constant, $\sigma_{x,y,z}$ are the standard deviations of the Gaussian distribution in the three spatial directions, and $z(t)$ is the distance between the probe-generated electron and the space charge distribution. Following Oloff et al.'s works,[12,13] the electron cloud spatial expansion was taken into account using a correction linearly dependent on the cloud velocity. In eq 2, the number of holes on the surface (mirror charge) can be written as

$$N^+(t) = X \cdot N^- \cdot e^{-t/\tau} \quad (3)$$

where X is the fraction of holes that survive rapid recombination such as Auger recombination and τ is the hole recombination time constant in the material. For negative delay times (i.e., when the probe pulse reaches the sample before the pump pulse), the photogenerated hole distribution is assumed to be completely screened by the pump-electron cloud, so $V^+(z(t \le 0)) = 0$.

Figure 1a reports an example of the PES valence band spectra of the CeO_2 sample at a positive (100 ps) and a negative (−100 ps) delay time with the pump at 4.1 eV as well as a reference spectrum acquired without the pump. The spectra were acquired with a HHG probe at 31.2 eV (13th harmonics). The spectra show an intense and broad peak between 7 and 4 eV (binding energy (BE)) due to emissions from the valence band of the O 2p character and a less intense peak between 3 and 1 eV due to emissions from occupied Ce 4f levels. At positive (negative) delay times, the spectrum appears rigidly shifted toward lower (higher) kinetic energies, with respect to the reference spectrum. The energy shift of the spectrum is the combination of the effects of space charge, which shifts the spectrum toward higher kinetic energies, and mirror charge, which shifts the spectrum in the opposite direction. The spectra, at the delay times that have been considered for the analysis (i.e., for $|t| \gtrsim 15$ ps), only show a rigid shift in kinetic energy while their shape is unaltered (see Figure S2 in the Supporting Information, SI). For this reason, the PES intensity within a fixed kinetic energy window, centered where the spectrum intensity shows large variations, e.g., at the top of the valence band, can be directly correlated to the energy shift of the spectra (red box in Figure 1a). We thus restricted the acquisition to an energy window of 1 eV width, centered at 4 eV. In this way, we can acquire fast and repeatable measurements, rapidly improving the statistics in relatively stable conditions.

https://doi.org/10.1021/acs.jpcc.2c02148
J. Phys. Chem. C 2022, 126, 11174−11181

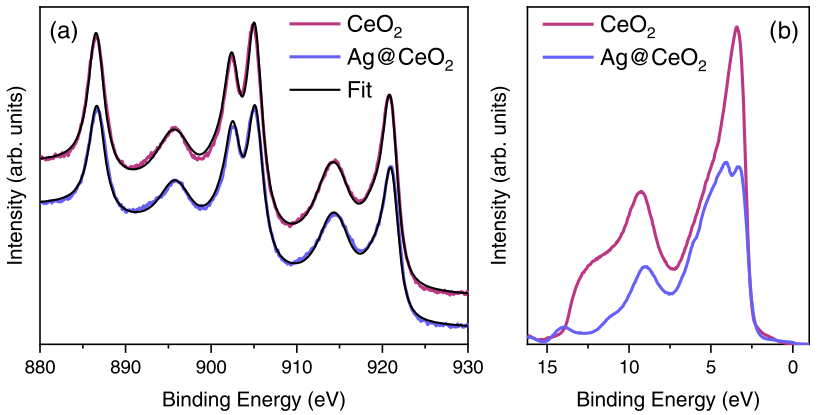

Figure 2. (a) XPS Ce 3d spectra of CeO_2 (red) and Ag@CeO_2 (green) with Al Kα photon energy (1486 eV). The black lines are the fits of the spectra using Ce^{4+}- and Ce^{3+}-related components. (b) UPS spectra of CeO_2 (red) and Ag@CeO_2 (green) at a photon energy of 21.2 eV.

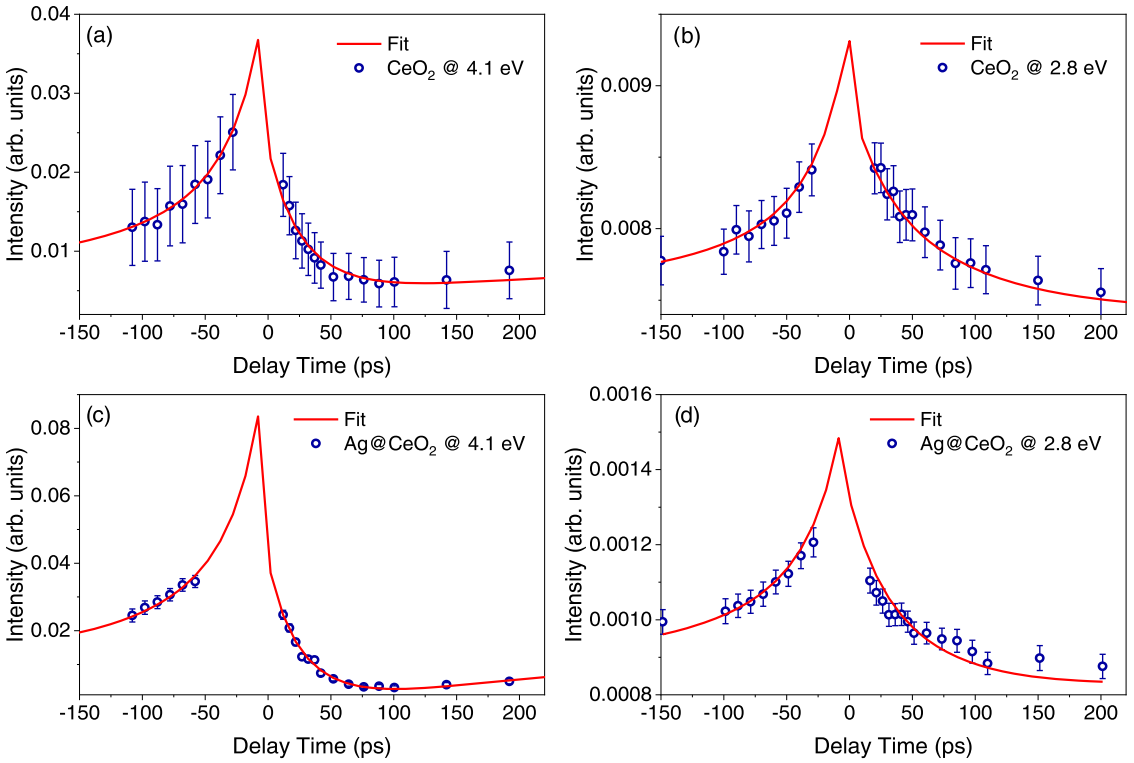

Figure 3. PES area intensity within the chosen energy for the CeO_2 sample pumped (a) above (4.1 eV) and (b) below (2.8 eV) the band gap as a function of delay time (blue dots). The dynamics were obtained using a HHG probe of 31.2 eV for panels (a, d) and 26.5 eV for panels (b, c). Panels (c, d) show the intensity for Ag@CeO_2 pumped above (4.1 eV) and below (2.8 eV) the CeO_2 band gap. Panel (c) is obtained using a HHG probe of 26.5 eV, while panel (d) is obtained using a HHG probe of 31.2 eV.

The valence band spectra shown in Figure 1 were modeled using three Gaussians, two to reproduce the O 2p and one for the Ce 4f peak (details in the SI; Figures S3 and S4). For each Gaussian, the kinetic energy shift $\mu(t)$, generated by the space charge and calculated using eq 1, can be related to the integral of the measured PES intensity in the chosen energy interval by

$$J^{(i)}(t) = I_0^{(i)} \cdot \int_{E_1}^{E_2} e^{-(E-\mu_0^{(i)}-\mu(t))^2/\sigma_0^{(i)2}} \cdot dE \quad (4)$$

where $\mu_0^{(i)}$, $I_0^{(i)}$, and $\sigma_0^{(i)}$ represent, respectively, the position of the centroid, the intensity, and the variance of the ith Gaussian in the spectrum acquired without the pump (evaluated from the fit of the full PES spectra reported in the SI; Figures S3 and S4) and E_1 and E_2 are the extremes of the chosen energy interval. The overall intensity integral variation, as a function of delay time between the pump and the probe pulses, is given by the sum

$$J(t) = J^{(1)}(t) + J^{(2)}(t) + J^{(3)}(t) \quad (5)$$

The PES intensity, measured within the chosen energy window, as a function of the delay time was fit using eq 4. The fitting variables were N^- (the number of photogenerated electrons), X (the fraction of holes in the sample), and τ (the hole recombination time constant). The x and y dimensions of the electron cloud for eq 2 at $t = 0$ were derived from the size of the spot on the sample (about 300 μm of FWHM),[26] while the z dimension was fixed to tens of nanometers. The number of pump-generated electrons N^- is compared with that of the

https://doi.org/10.1021/acs.jpcc.2c02148
J. Phys. Chem. C 2022, 126, 11174−11181

Table 1. Hole Lifetime, Fraction of Excited Holes (Obtained from the Fitting of the Data in Figure 3), and Measured Drain Current for the CeO_2 and Ag@CeO_2 Samples at the Two Different Pumps (4.1 eV above the CeO_2 Gap and 2.8 eV below)[a]

sample	pump (eV)/fluence (μJ)	hole lifetime (ps)	fraction of holes X	N^-	drain current (pA)
CeO_2	4.1/0.7	150	0.46	2700	104 (2.6 10^4 carriers)
	2.8/0.9	87	0.29	140	27 (6.7 10^3 carriers)
Ag@CeO_2	4.1/0.7	153	0.54	6500	600 (1.5 10^5 carriers)
	2.8/1	300	0.35	1900	320 (8 10^4 carriers)

[a]The values of the drain current are normalized to the laser frequency.

drain current, as reported in Table 1. However, only in the case of the CeO_2 sample pumped below the gap, the current is close to the limit conditions for the validity of the model, being just 1 order of magnitude higher than the probe-generated one.

RESULTS AND DISCUSSION

In situ XPS and UPS measurements have been acquired after sample growth to obtain information on the surface electronic structure of the samples. The Ce 3d XPS spectra of the two samples show a line shape compatible with a dominant CeO_2 stoichiometry, confirmed by the good quality of the fit obtained using only Ce^{4+}-related components (Figure 2a). The Ce^{3+} concentration is therefore below the sensitivity of the technique, as observed for ultrathin films grown in similar conditions.[17,20] The UPS spectra of the two samples, reported in Figure 2b, show a broad feature between 2 and 5 eV assigned to the valence band with the O 2p character. The minor differences in shape as compared to the spectra shown in Figure 1 can be ascribed to the difference in photon energy between the UPS lamp, 21.2 eV, and the HHG at the SPRINT facility (26.5 and 31.2 eV). In the Ag@CeO_2 sample, the O 2p-related main feature around 3 eV is attenuated in intensity as compared to the CeO_2 sample and Ag-related features around 5 eV and at the Fermi level.[23] The absence of valence band features related to the metallic substrates confirms the complete coverage of the substrate surface by the oxide films.

The samples investigated here are grown on highly reflective metal single crystals, which do not easily allow for optical characterization. A sample grown on a transparent MgO substrate with the same procedures and the same Ag nominal thickness shows a very broad LSPR-related absorption band in the visible.[23] Thus, in analogy with previous experiments made on these systems,[2,4] the trPES measurements have been acquired on the CeO_2 and the Ag@CeO_2 samples using two different pumps: one at 4.1 eV, above the CeO_2 band gap, and one at 2.8 eV, at the Ag LSPR maximum and below the CeO_2 band gap. The trPES data for each pump and delay time have been acquired in the 1 eV energy window centered at the top of the valence band, as described in the Methods section. Figure 3 shows the area of the PES intensity J in the selected window with respect to that of the spectrum without the pump as a function of delay time (blue dots) for the two different samples and the two pump energies. The differences in the error bar intensities depend on the statistics (the number of acquisitions).

The acquisition was limited to delay times larger than $|t| \gtrsim 15$ ps (and up to 200 ps) for which the valence band spectrum did not show evident deformations (see SI Figure S2). Unfortunately, this limitation prevents the detection of ultrafast dynamic decays, often observed in oxides after band-gap excitation.[28,29] At negative delay times, J shows an increasing intensity as the delay time approaches zero for both samples and pump energies. The observed behavior agrees with a progressive shift of the spectra toward higher kinetic energies with decreasing $|\Delta t|$ because of the pump-generated space charge. The effect of the positive potential generated by the holes left in the sample, which are screened by the pump-generated electron cloud, is in fact negligible, as assumed by the model described in the Methods section. At positive delay times, the two samples pumped above the band gap (Figure 3a,c) show a marked decrease (faster than the rise time at negative delays) and then, at delays longer than 100 ps, a slower increase of J, indicating that for positive delay times both space and mirror charge contributions are simultaneously at play. The rapid decrease of $J(t)$ is due to the shift toward lower kinetic energies induced by the positive mirror charge, which dominates at short delay times,[10,12] while this is partially compensated by the presence of the space charge at longer delay times. At longer delay times, $J(t)$ should tend to the same values; however, our temporal window was not wide enough to reach that condition. Similar behavior is observed at positive delays also for the Ag@CeO_2 sample with the pump at the LSPR (Figure 3d), although in this case, the variation with respect to negative delays is less pronounced, in agreement with a lower density of holes generated in the sample in this case. The CeO_2 sample pumped below the band gap instead shows an almost symmetric behavior at positive and negative delay times (Figure 3b). This is consistent with a fast recombination and with the expected very low density of holes formed in this sample, which has an extremely low absorbance at 2.8 eV.[2]

Following the model presented in the Methods section, the data in Figure 3 were fit using eq 4. The fitting curves obtained are reported as red lines in the figure. The free fitting parameters, reported for each sample and pump energy in Table 1, are the fraction X of excited holes, their lifetime τ, and the number of photogenerated electrons N^-. The Gaussian functions, which describe the PES for each probe energy and for each sample, are reported in the SI Figures S3 and S4.

The analysis of the space charge effect gives relevant information on the dynamics of charge recombination in the material, in particular, on pump-induced holes, within the investigated time-scale range. The ultrathin films used for the present experiment are grown on metallic substrates, and the Fermi level of the sample is at equilibrium with that of the experimental apparatus connected to the ground. The correlation between the space charge effect and the drain current is evident by comparing the values of current and the N^- factor extracted by the fit (Table 1). The pump excitation leads to the formation of holes on the surface of the samples induced by different processes. The fitting procedure makes it possible to extract information on the compensation of such holes by the drain current from the ground and to infer important properties of the material based on the observed behavior.

https://doi.org/10.1021/acs.jpcc.2c02148
J. Phys. Chem. C 2022, 126, 11174−11181

The increase in electron yield in the presence of Ag NPs (Table 1) is partially caused by the direct emission of electrons from the NPs into the vacuum through multiphoton processes at both 4.1 and 2.8 eV, although the latter energy is expected to be less efficient (considering that the intensity of the two pumps is low and similar). For this reason, we expect that the photoemission from defect levels should play a predominant role in the space charge formation. The Ag insertion in the CeO_2 matrix should increase the density of defects in the oxide matrix.

As reported in Table 1, the band-gap excitation by the 4.1 eV pump leads to the formation of a large fraction of holes with a lifetime on the order of 100 ps on both samples. The fraction of estimated mirror charges and their lifetime does not show significant changes if Ag NPs are introduced into the oxide film since at this pump energy the holes are mainly formed within the oxide film. This is a further confirmation of the fact that the two films have comparable properties in spite of the different substrates used. This can be rationalized by considering that charge reneutralization by electrons from the grounded substrate most likely takes place not only at ideal interface sites (film/substrate) overcoming the Schottky barrier but mainly along domain boundaries and defect sites. Although the pump wavelength of 4.1 eV is energetic enough to excite interband transitions in the Ag NPs, these are expected to have a lower cross section and to decay much more rapidly, compared to the above-band-gap excitation in the surrounding oxide,[4] thus having a negligible effect on the photoelectrons at delay times longer than 15 ps. A lifetime for the holes above 100 ps, determined from trPES measurements, is consistent with the persistence of the ground-state bleaching feature for hundreds of picoseconds, observed in the same systems by femtosecond transient absorption spectroscopy after the above-band-gap excitation.[4] Some other oxides, like TiO_2 in the form of single crystals with low defect concentrations, show comparatively long lifetimes of photo-excited states.[30,31] On the other hand, hole lifetimes on the order of a few picoseconds have been reported for Fe_2O_3 thin films unless trapping states are involved.[32]

In contrast, the results obtained with a pump at 2.8 eV are quite different. As reported in Table 1, in the CeO_2 sample, a small fraction of holes is detected, with a lifetime of less than 100 ps. These mainly generate the excitation of low-density defect sites but cannot exclude the multiphotonic absorption. The holes recombine in less than 100 ps, with electrons coming from the grounded metallic substrate, expected to propagate via hopping or through CeO_2 defects like domain boundaries. When Ag NPs are introduced, the efficiency of carrier generation increases by more than 1 order of magnitude (see drain currents and N^- values reported in Table 1). This can be related to the increased defect density generated at the interface between CeO_2 and the Ag NPs and to the excitation of LSPRs, which introduces a significant perturbation in the system. The fraction of excited holes is comparable to the case of the CeO_2 film (Table 1); however, the mirror charges persist for significantly longer lifetimes of several hundreds of picoseconds, i.e., above the considered delay time. The significantly higher lifetime, observed in Ag@CeO_2 with a 2.8 eV pump, can be qualitatively explained by considering that a high number of positive carriers are formed at this energy on the NP surface due to the injection of electrons, stemming from the LSPR decay, into CeO_2. The sketch in Figure 4 summarizes the processes that are expected to occur. At an excitation energy of 4.1 eV, the holes on the NPs are mainly generated by defects and multiphotonic photoemission (Figure 4a), while using a 2.8 eV pulse, the holes are expected to be mainly generated by plasmon-mediated electron injection into CeO_2 (Figure 4b). Most of the carriers formed in the Ag NPs after LSPR de-excitation survives for relatively long times due to the presence of a Schottky barrier between the NPs and the oxide, which prevents their recombination with electrons injected into the oxide. The corresponding injected electrons possibly compensate the holes directly formed on the oxide within shorter times, leading to a situation in which most of the unscreened positive charge is located on the NP surface within relatively short times (certainly well below 15 ps) from excitation (Figure 4c). On the contrary, at 2.8 eV in the CeO_2 film, the holes due to defect state absorption are neutralized by means of fast nonradiative recombination with the electrons from the substrate. The mirror charge lifetimes resulting from the fit are related to the decay of the populations of the positive charges in the NPs and in CeO_2. Thus, the significantly different lifetimes extracted for the excitation at 2.8 eV for the CeO_2 sample (87 ps) and Ag@CeO_2 (300 ps) agree with the expected longer reneutralization times of the positive carriers generated in the metal NPs as compared to the holes present in CeO_2.

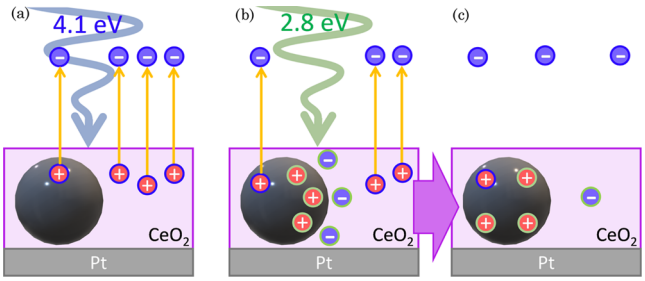

Figure 4. Sketch of the processes that dominate at different pump energies for the Ag@CeO_2 sample. (a) The pump at 4.1 eV induces the formation of holes both in the NPs and in the oxide by defect states and multiphoton-induced photoemission; (b) the pump at 2.8 eV induces the formation of a few holes in the oxide and in the NPs by multiphoton-induced photoemission (blue contours) and of a relevant number of holes on the NPs via plasmon-mediated electron injection from the NP to the oxide (green contour); (c) the electrons and holes in the oxide recombine within short times (<15 ps), leaving a relevant fraction of uncompensated positive charges on the NP surface.

A further consideration that can be made based on the results obtained is that even the positive carriers generated after LSPR excitation in the Ag NPs recombine within a few hundreds of picoseconds, preventing the accumulation of charges, which would hinder further electron injection to the oxide. This is a relevant aspect for an effective application of CeO_2 combined with plasmonic NPs as an efficient visible light photocatalyst. In previous works by the authors,[4,8] based on ultrafast optical UV−vis and XUV spectroscopies, it was shown that either during or after the excitation of the LSPR in the Ag NPs there is significant efficiency of injection of electrons from the Ag into CeO_2. This process was shown to occur on a time scale of fewer than 200 fs, which is well below the temporal window available in the present experiment. However, the dynamics of the neutralization of the positive charges (holes) in the Ag NPs could not be easily studied using the techniques employed in the previous works. The approach here used allows us to isolate the effect of photogenerated holes, which

https://doi.org/10.1021/acs.jpcc.2c02148
J. Phys. Chem. C 2022, 126, 11174−11181

play a relevant role in the functionality of the investigated system.

CONCLUSIONS

The present work exploits the space charge effect in time-resolved photoelectron spectroscopy to gain information on the dynamics of photoexcited holes in a cerium oxide film, also in combination with plasmonic Ag nanoparticles on time scales above 15 ps. We have applied a procedure that makes it possible to significantly reduce the acquisition times, allowing an increase in the number of samples and pump energies to be investigated in a single experiment. More importantly, the analysis of the time-resolved photoemission spectra allowed us to infer that the above-band-gap excitation in cerium oxide leads to the formation of holes with lifetimes exceeding 100 ps, independent of the presence of Ag nanoparticles. The sub-band-gap excitation, on the other hand, results in the formation of holes with lifetimes on the order of a few tens of picoseconds in CeO_2, possibly induced by defect-related transitions or multiphoton absorption. Interestingly, when the oxide is coupled with Ag nanoparticles, the excitation of the sub-band-gap localized surface plasmon resonance leads to the formation of positive charges in the metal with lifetimes exceeding 300 ps. This study represents an example of how to exploit the space charge effect in gaining access to the carrier dynamics in the CeO_2-based materials within the picosecond range of time, which is fundamental to describe the photocatalytic processes.

ASSOCIATED CONTENT

Supporting Information

The Supporting Information is available free of charge at https://pubs.acs.org/doi/10.1021/acs.jpcc.2c02148.

Comparison of CeO_2 and Ag@CeO_2 photoemission spectra acquired with the HHG; modification of the PE spectra induced by the space charge in the first 20 ps; and the steady spectra fitting procedure is presented together with the results (PDF)

AUTHOR INFORMATION

Corresponding Author

Jacopo Stefano Pelli Cresi − *Elettra-Sincrotrone Trieste, 34012 Basovizza, Trieste, Italy;* orcid.org/0000-0001-6437-7411; Email: jacopo.pellicresi@iit.it

Authors

Eleonora Spurio − *Dipartimento FIM, Università degli Studi di Modena e Reggio Emilia, 41125 Modena, Italy; Istituto Nanoscienze - CNR-NANO, 41125 Modena, Italy*

Lorenzo Di Mario − *Istituto di Struttura della Materia - CNR (ISM-CNR), EuroFEL Support Laboratory (EFSL), 00133 Rome, Italy; Zernike Institute for Advanced Materials, University of Groningen, Groningen 9747 AG, The Netherlands*

Patrick O'Keeffe − *Istituto di Struttura della Materia - CNR (ISM-CNR), EuroFEL Support Laboratory (EFSL), Monterotondo Scalo 00015, Italy;* orcid.org/0000-0002-8676-4436

Stefano Turchini − *Istituto di Struttura della Materia - CNR (ISM-CNR), EuroFEL Support Laboratory (EFSL), 00133 Rome, Italy*

Stefania Benedetti − *Istituto Nanoscienze - CNR-NANO, 41125 Modena, Italy;* orcid.org/0000-0002-2683-4818

Gian Marco Pierantozzi − *Istituto Officina dei Materiali-CNR Laboratorio TASC, Trieste I-34149, Italy;* orcid.org/0000-0002-5044-5716

Alessandro De Vita − *Istituto Officina dei Materiali-CNR Laboratorio TASC, Trieste I-34149, Italy*

Riccardo Cucini − *Istituto Officina dei Materiali-CNR Laboratorio TASC, Trieste I-34149, Italy*

Daniele Catone − *Istituto di Struttura della Materia - CNR (ISM-CNR), EuroFEL Support Laboratory (EFSL), 00133 Rome, Italy;* orcid.org/0000-0002-7649-2756

Paola Luches − *Istituto Nanoscienze - CNR-NANO, 41125 Modena, Italy;* orcid.org/0000-0003-1310-5357

Complete contact information is available at: https://pubs.acs.org/10.1021/acs.jpcc.2c02148

Author Contributions

[▽]D.C. and P.L. contributed equally to this work.

Author Contributions

E.S., S.B., and P.L.: sample preparation and in situ characterization; J.P.C., E.S., L.D.M., S.T., G.M.P., A.D.V., R.C., and D.C.: HHG pump−probe experiment; J.P.C. and E.S.: methodology; all authors: writing the original draft and the writing review; J.P.C.: editing preparation; and D.C. and P.L.: supervision.

Notes

The authors declare no competing financial interest.

ACKNOWLEDGMENTS

The authors would like to thank Riccardo Mincigrucci and Dario De Angelis for the fruitful discussion of the data analysis. This work was performed in the framework of the Nanoscience Foundry and Fine Analysis (NFFA-MIUR Italy Progetti Internazionali) facility.

REFERENCES

(1) Melchionna, M.; Fornasiero, P. Sustainability and Nanomaterials in Concert. *ChemCatChem* **2017**, *9*, 3274−3284.

(2) Cresi, J. S. P.; Di Mario, L.; Catone, D.; Martelli, F.; Paladini, A.; Turchini, S.; D'Addato, S.; Luches, P.; O'Keeffe, P. Ultrafast Formation of Small Polarons and the Optical Gap in CeO2. *J. Phys. Chem. Lett.* **2020**, *11*, 5686−5691.

(3) Yoshihara, T.; Katoh, R.; Furube, A.; Tamaki, Y.; Murai, M.; Hara, K.; Murata, S.; Arakawa, H.; Tachiya, M. Identification of Reactive Species in Photoexcited Nanocrystalline TiO2 Films by Wide-Wavelength-Range (400−2500 Nm) Transient Absorption Spectroscopy. *J. Phys. Chem. B* **2004**, *108*, 3817−3823.

(4) Cresi, J. S. P.; Spadaro, M. C.; D'Addato, S.; Valeri, S.; Benedetti, S.; Bona, A. D.; Catone, D.; Mario, L. D.; O'Keeffe, P.; Paladini, A.; et al. Highly Efficient Plasmon-Mediated Electron Injection into Cerium Oxide from Embedded Silver Nanoparticles. *Nanoscale* **2019**, *11*, 10282−10291.

(5) Xu, Z.; Lin, Y.; Yin, M.; Zhang, H.; Cheng, C.; Lu, L.; Xue, X.; Fan, H. J.; Chen, X.; Li, D. Understanding the Enhancement Mechanisms of Surface Plasmon-Mediated Photoelectrochemical Electrodes: A Case Study on Au Nanoparticle Decorated TiO2 Nanotubes. *Adv. Mater. Interfaces* **2015**, *2*, No. 1500169.

(6) Clavero, C. Plasmon-Induced Hot-Electron Generation at Nanoparticle/Metal-Oxide Interfaces for Photovoltaic and Photocatalytic Devices. *Nat. Photonics* **2014**, *8*, 95−103.

(7) Wu, N. Plasmonic Metal−Semiconductor Photocatalysts and Photoelectrochemical Cells: A Review. *Nanoscale* **2018**, *10*, 2679−2696.

(8) Cresi, J. S. P.; Principi, E.; Spurio, E.; Catone, D.; O'Keeffe, P.; Turchini, S.; Benedetti, S.; Vikatakavi, A.; D'Addato, S.; Mincigrucci, R.; et al. Ultrafast Dynamics of Plasmon-Mediated Charge Transfer in Ag@CeO2 Studied by Free Electron Laser Time-Resolved X-Ray Absorption Spectroscopy. *Nano Lett.* **2021**, *21*, 1729−1734.
(9) Oura, M.; Wagai, T.; Chainani, A.; Miyawaki, J.; Sato, H.; Matsunami, M.; Eguchi, R.; Kiss, T.; Yamaguchi, T.; Nakatani, Y.; et al. Development of a Single-Shot CCD-Based Data Acquisition System for Time-Resolved X-Ray Photoelectron Spectroscopy at an X-Ray Free-Electron Laser Facility. *J. Synchrotron Radiat.* **2014**, *21*, 183−192.
(10) Zhou, X. J.; Wannberg, B.; Yang, W. L.; Brouet, V.; Sun, Z.; Douglas, J. F.; Dessau, D.; Hussain, Z.; Shen, Z.-X. Space Charge Effect and Mirror Charge Effect in Photoemission Spectroscopy. *J. Electron Spectrosc. Relat. Phenom.* **2005**, *142*, 27−38.
(11) Hellmann, S.; Rossnagel, K.; Marczynski-Bühlow, M.; Kipp, L. Vacuum Space-Charge Effects in Solid-State Photoemission. *Phys. Rev. B* **2009**, *79*, No. 035402.
(12) Oloff, L.-P.; Hanff, K.; Stange, A.; Rohde, G.; Diekmann, F.; Bauer, M.; Rossnagel, K. Pump Laser-Induced Space-Charge Effects in HHG-Driven Time- and Angle-Resolved Photoelectron Spectroscopy. *J. Appl. Phys.* **2016**, *119*, No. 225106.
(13) Oloff, L.-P.; Chainani, A.; Matsunami, M.; Takahashi, K.; Togashi, T.; Osawa, H.; Hanff, K.; Quer, A.; Matsushita, R.; Shiraishi, R.; et al. Time-Resolved HAXPES Using a Microfocused XFEL Beam: From Vacuum Space-Charge Effects to Intrinsic Charge-Carrier Recombination Dynamics. *Sci. Rep.* **2016**, *6*, No. 35087.
(14) Passlack, S.; Mathias, S.; Andreyev, O.; Mittnacht, D.; Aeschlimann, M.; Bauer, M. Space Charge Effects in Photoemission with a Low Repetition, High Intensity Femtosecond Laser Source. *J. Appl. Phys.* **2006**, *100*, No. 024912.
(15) Al-Obaidi, R.; Wilke, M.; Borgwardt, M.; Metje, J.; Moguilevski, A.; Engel, N.; Tolksdorf, D.; Raheem, A.; Kampen, T.; Mähl, S.; et al. F. Ultrafast Photoelectron Spectroscopy of Solutions: Space-Charge Effect. *New J. Phys.* **2015**, *17*, No. 093016.
(16) Verna, A.; Stefani, G.; Offi, F.; Gejo, T.; Tanaka, Y.; Tanaka, K.; Nishie, T.; Nagaya, K.; Niozu, A.; Yamamura, R.; et al. Photoemission from the Gas Phase Using Soft X-Ray Fs Pulses: An Investigation of the Space-Charge Effects. *New J. Phys.* **2020**, *22*, No. 123029.
(17) Staudt, T.; Lykhach, Y.; Hammer, L.; Schneider, M. A.; Matolín, V.; Libuda, J. A Route to Continuous Ultra-Thin Cerium Oxide Films on Cu(111). *Surf. Sci.* **2009**, *603*, 3382−3388.
(18) Grinter, D. C.; Ithnin, R.; Pang, C. L.; Thornton, G. Defect Structure of Ultrathin Ceria Films on Pt(111): Atomic Views from Scanning Tunnelling Microscopy. *J. Phys. Chem. C* **2010**, *114*, 17036−17041.
(19) Luches, P.; Pagliuca, F.; Valeri, S.; Boscherini, F. Structure of Ultrathin CeO2 Films on Pt(111) by Polarization-Dependent X-Ray Absorption Fine Structure. *J. Phys. Chem. C* **2013**, *117*, 1030−1036.
(20) Luches, P.; Pagliuca, F.; Valeri, S. Morphology, Stoichiometry, and Interface Structure of CeO2 Ultrathin Films on Pt(111). *J. Phys. Chem. C* **2011**, *115*, 10718−10726.
(21) Benedetti, F.; Luches, P.; Spadaro, M. C.; Gasperi, G.; Daddato, S.; Valeri, S.; Boscherini, F. Structure and Morphology of Silver Nanoparticles on the (111) Surface of Cerium Oxide. *J. Phys. Chem. C* **2015**, *119*, 6024−6032.
(22) Hu, S.; Wang, Y.; Wang, W.; Han, Y.; Fan, Q.; Feng, X.; Xu, Q.; Zhu, J. Ag Nanoparticles on Reducible CeO2(111) Thin Films: Effect of Thickness and Stoichiometry of Ceria. *J. Phys. Chem. C* **2015**, *119*, 3579−3588.
(23) Cresi, J. S. P.; Silvagni, E.; Bertoni, G.; Spadaro, M. C.; Benedetti, S.; Valeri, S.; D'Addato, S.; Luches, P. Optical and Electronic Properties of Silver Nanoparticles Embedded in Cerium Oxide. *J. Chem. Phys.* **2020**, *152*, No. 114704.
(24) Skála, T.; Šutara, F.; Prince, K. C.; Matolín, V. Cerium Oxide Stoichiometry Alteration via Sn Deposition: Influence of Temperature. *J. Electron Spectrosc. Relat. Phenom.* **2009**, *169*, 20−25.
(25) Open access is performed through the NFFA-SPRINT web site. *NFFA-Trieste*. https://www.trieste.nffa.eu/ (accessed 2022-02-28).
(26) Cucini, R.; Pincelli, T.; Panaccione, G.; Kopic, D.; Frassetto, F.; Miotti, P.; Pierantozzi, G. M.; Peli, S.; Fondacaro, A.; De Luisa, A.; et al. Coherent Narrowband Light Source for Ultrafast Photoelectron Spectroscopy in the 17−31 EV Photon Energy Range. *Struct. Dyn.* **2020**, *7*, No. 014303.
(27) Kheifets, S. *Potential of a Three-Dimensional Gaussian Bunch*; PUBDB-2017-01789; Bibliothek und Dokumentation, 1976.
(28) Garcia, J. M.; Heald, L. F.; Shaffer, R. E.; Sayres, S. G. Oscillation in Excited State Lifetimes with Size of Sub-Nanometer Neutral (TiO2)n Clusters Observed with Ultrafast Pump−Probe Spectroscopy. *J. Phys. Chem. Lett.* **2021**, *12*, 4098−4103.
(29) Zhang, Y.; Payne, D. T.; Pang, C. L.; Cacho, C.; Chapman, R. T.; Springate, E.; Fielding, H. H.; Thornton, G. State-Selective Dynamics of TiO2 Charge-Carrier Trapping and Recombination. *J. Phys. Chem. Lett.* **2019**, *10*, 5265−5270.
(30) Yamada, Y.; Kanemitsu, Y. Determination of Electron and Hole Lifetimes of Rutile and Anatase TiO2 Single Crystals. *Appl. Phys. Lett.* **2012**, *101*, No. 133907.
(31) Xu, M.; Gao, Y.; Moreno, E. M.; Kunst, M.; Muhler, M.; Wang, Y.; Idriss, H.; Wöll, C. Photocatalytic Activity of Bulk TiO2 Anatase and Rutile Single Crystals Using Infrared Absorption Spectroscopy. *Phys. Rev. Lett.* **2011**, *106*, No. 138302.
(32) Joly, A. G.; Williams, J. R.; Chambers, S. A.; Xiong, G.; Hess, W. P.; Laman, D. M. Carrier Dynamics in A-Fe2O3 (0001) Thin Films and Single Crystals Probed by Femtosecond Transient Absorption and Reflectivity. *J. Appl. Phys.* **2006**, *99*, No. 053521.

Recommended by ACS

Charge Separation, Band-Bending, and Recombination in WO_3 Photoanodes
Sacha Corby, James R. Durrant, *et al.*
AUGUST 16, 2019
THE JOURNAL OF PHYSICAL CHEMISTRY LETTERS
READ

Reduced Recombination and Capacitor-like Charge Buildup in an Organic Heterojunction
Kyra N. Schwarz, Kenneth P. Ghiggino, *et al.*
JANUARY 10, 2020
JOURNAL OF THE AMERICAN CHEMICAL SOCIETY
READ

Energy-Temporal Pathways of Free-Charge Formation at Organic Bilayers: Competition of Delocalization, Disorder, and Polaronic Effects
Veljko Janković and Nenad Vukmirović
FEBRUARY 03, 2020
THE JOURNAL OF PHYSICAL CHEMISTRY C
READ

Probing Charge Generation Efficiency in Thin-Film Solar Cells by Integral-Mode Transient Charge Extraction
Stefan Zeiske, Ardalan Armin, *et al.*
MARCH 31, 2022
ACS PHOTONICS
READ

Get More Suggestions >